Hindawi Publishing Corporation
International Journal of Photoenergy
Volume 2014, Article ID 783531, 7 pages
http://dx.doi.org/10.1155/2014/783531

Research Article

Fabrication and Characteristics of Macroporous TiO_2 Photocatalyst

Guiyun Yi,[1] Baolin Xing,[1] Jianbo Jia,[1] Liwei Zhao,[2] Yuanfeng Wu,[1] Huihui Zeng,[1] and Lunjian Chen[1]

[1] *School of Materials Science and Engineering, Henan Polytechnic University, Jiaozuo, Henan 454000, China*
[2] *Petroleum Engineering Research Institute of Dagang Oilfield, Tianjin 300270, China*

Correspondence should be addressed to Guiyun Yi; ygyun@hpu.edu.cn and Lunjian Chen; lunjianc@hpu.edu.cn

Received 5 February 2014; Accepted 26 February 2014; Published 20 March 2014

Academic Editor: Jianliang Cao

Macroporous TiO_2 photocatalyst was synthesized by a facile nanocasting method using polystyrene (PS) spherical particles as the hard template. The synthesized photocatalyst was characterized by transmission electron microscope (TEM), scanning electron microscopy (SEM), thermogravimetry-differential thermogravimetry (TG-DTG), X-ray diffraction (XRD), and N_2-sorption. TEM, SEM, and XRD characterizations confirmed that the macroporous TiO_2 photocatalyst is composed of anatase phase. The high specific surface area of 87.85 m^2/g can be achieved according to the N_2-sorption analysis. Rhodamine B (RhB) was chosen as probe molecule to evaluate the photocatalytic activity of the TiO_2 catalysts. Compared with the TiO_2 materials synthesized in the absence of PS spherical template, the macroporous TiO_2 photocatalyst sintered at 500°C exhibits much higher activity on the degradation of RhB under the UV irradiation, which can be assigned to the well-structured macroporosity. The macroporous TiO_2 material presents great potential in the fields of environmental remediation and energy conversion and storage.

1. Introduction

For the environment protection purpose, the disposal of various toxic dyes from the textile industry has attracted extensive attention. Rhodamine B (RhB) is widely used as a colorant in textiles and food stuffs and is also a well-known water tracer fluorescent [1]. It is harmful to human beings and animals and causes irritation of the skin, eyes, and respiratory tract.

Owing to high photocatalytic efficiency, good oxidation capability, stable chemical reaction, low cost, and nontoxicity, titanium dioxide (TiO_2) has been applied widely in wastewater treatment [2–4], environment purification [5, 6], solar energy transfer [7, 8], chemical sensing [9, 10]. Recently, it was found that incorporation of well-defined porosity of TiO_2 materials could greatly enhance the photoactivity in the area of environmental remediation and energy conversion [11–13]. For a variety of practical applications, the fabrication of desired structure with network is important as well as control in grain size, crystallinity, and composition [14–16].

At present, porous TiO_2, combining the outstanding properties of TiO_2 with their porous structure, has gained great research interests, and various synthetic techniques had been developed. For example, Liu et al. prepared anatase TiO_2 porous thin films by sol-gel method with CTAB surfactant as a pore-forming agent, and many factors were studied [17]. Bala et al. fabricated hollow spheres of anatase TiO_2 by spherical $CaCO_3$ nanoparticles as a template and investigated the photocatalytic activity [18]. Zheng et al. synthesized rutile and anatase TiO_2 mesoporous single crystals with diverse mophologies by silica-templated hydrothermal method [19]. Dong et al. prepared highly ordered transparent TiO_2 macropore arrays via a glass-clamping method and investigated the potential application in degradation of organic dyes [20]. However, the general synthesis usually involved complicated multistep to obtain porous skeleton. Firstly, it is required to assemble spheres into colloidal crystals as templates, and then the precursor is filled into interstices among the crystals for several times [21–23]. Moreover, for an efficient photodegradation catalyst, the macroporous structure is essential due

to the run-through-macropore network which maximizes the uptake and the diffusion of the organic molecules [24–26]. Additionally, the porous structures are propitious to enhance the light scattering and improve the utilization rate of irradiation light [27–29].

Herein, a simple method without assembly and filling steps was introduced in this work for the preparation of macroporous TiO_2 through a sol-gel process using polystyrene spheres as sacrificial templates. Compared with the TiO_2 materials synthesized in the absence of PS spherical template [30, 31], the macroporous TiO_2 photocatalyst sintered at 500°C exhibits much higher activity on the degradation of RhB under the UV irradiation. The macroporous TiO_2 material present great potential in the fields of environmental remediation and energy conversion and storage.

2. Experiment

2.1. Materials. Tetrabutyl titanate ($Ti(OC_4H_9)_4$), sodium styrene sulfonate, sodium hydrogen carbonate, potassium persulfate, ethanol, Rhodamine B (RB), acetic acid, and nitric acid were all analytical grade and used without further purification. Styrene was washed by 5% NaOH solution several times to remove polymerization inhibitor. All of the reagents were purchased from Shanghai Chemical Reagent Ltd. Co.

2.2. Preparation of PS Microspheres. PS spheres were obtained by emulsion polymerization of styrene according to previous reports [32–34]. At first, 150 g deionized water was poured into a 300 mL jacket reactor, which was kept at 85°C until the end of the reaction. Then, 0.08 g sodium styrene sulfonate as the emulsifier and 0.0633 g sodium hydrogen carbonate as the buffer were dissolved in the deionized water. Under constant stirring, 18.30 mL styrene monomer was added to this solution, accompanied with nitrogen protection. After 1 h, 0.0833 g potassium persulfate as an initiator was introduced into the solution. After 18 h polymerization, the monodispersed PS spheres with the average diameter of 278 nm were obtained, and the standard deviation of spheres was less than 2.76%.

2.3. Preparation of TiO_2 Sol. With the $Ti(OC_4H_9)_4$ as precursor, ethanol as solvent and glacial acetic acid as inhibitor, TiO_2 sol was synthesized by sol-gel method according to references elsewhere [35, 36]. The procedure can be divided into three steps. At first, solution A was prepared by mixing 3 mL deionized water and 16 mL absolute ethyl alcohol. And then solution B was obtained by adding 10 mL $Ti(OC_4H_9)_4$ and 2 mL glacial acetic acid into 32 mL ethanol slowly with the rapid stirring. At last, solution A was dripped slowly into solution B under rapid stirring. The homogeneous and transparent solution of TiO_2 sol was thus obtained.

2.4. Preparation of Macroporous TiO_2. In a typical synthesis of macroporous TiO_2, 11 mL PS spheres suspension with the concentration of 5.88 wt% was added slowly into 10 mL as-prepared TiO_2 sol. The intimate mixture was obtained by stirring and ultrasonication. Then, the mixture was placed in an oven at 70°C for 12 h and then TiO_2/PS sphere composites were obtained. To prepare macroporous TiO_2, the as-obtained composites were sintered in muffle furnace at 500°C for 2 h in air. The ultima product was denoted as m-TiO_2. For contrast, the synthesis of TiO_2 nanoparticles was the similar to the preparation of macroporous TiO_2 without adding the PS spheres, which was labeled as r-TiO_2.

2.5. Characterization. Field emission scanning electron microscopy (FE-SEM) was carried out on FEI Sirion-200 and transmission electron microscopy TEM was taken on JEOL JEM-2100. The XRD patterns of the synthesized samples were obtained by a Bruker-AXS D8 Advance diffractometer with CuKα radiation (λ = 0.15418 nm). To determine the proper sintering temperature and analyze the weight content of PS spheres in the TiO_2/PS composites, both the as-prepared PS spheres and TiO_2/PS composites were investigated by thermogravimetry and derivative thermogravimetry (TG-DTG), which was operated at a program-controlled temperature elevation rate of 10°C/min in the air. N_2 adsorption-desorption isotherms were measured on a Quantachrome NOVA 2000e sorption analyzer at liquid nitrogen temperature (77 K). The samples were degassed at 120°C overnight prior to the measurement. The surface areas were calculated by the multipoint Brunauer-Emmett-Teller (BET) method.

2.6. Photocatalytic Experiment. The photocatalytic activity tests of the synthesized TiO_2 were performed by the degradation of Rhodamine B (RhB) under UV light irradiation under ambient conditions. The experiment was performed in a water-jacket reactor operated at 20°C. The light source was a 450 W high-pressure mercury lamp (Foshan Electrical and Lighting Co. Ltd.) with a strong peak centered at 362 nm. The distance between the sample and the lamp was about 10 cm. In a typical process, 0.1 g of the obtained product was placed into 100 mL of RhB aqueous solution (2×10^{-5} mol/L) under magnetic stirring. 5 mL of the mixture was collected at a given time interval of 15 min and was then centrifuged to discard any sediment. Then the concentration of RhB was determined on a TU-1810 UV-vis spectrophotometer at λ_{max} = 553 nm [37, 38]. The decomposition efficiency of RhB was calculated by the following formula:

$$\text{Decomposition efficiency} = \frac{A_0 - A_t}{A_0} \times 100\%, \quad (1)$$

where A_0 and A_t represent the absorbance of the RhB solution before irradiation and the absorbance at time t, respectively.

3. Results and Discussion

3.1. Material Characterization. TG-DTG curves of both PS spheres and the TiO_2/PS composites are shown in Figure 1. For PS spheres, three weight loss stages, below 300, 300–400, and 400–500°C, can be observed. The PS spheres undergo endothermic desorption of physically adsorbed water and

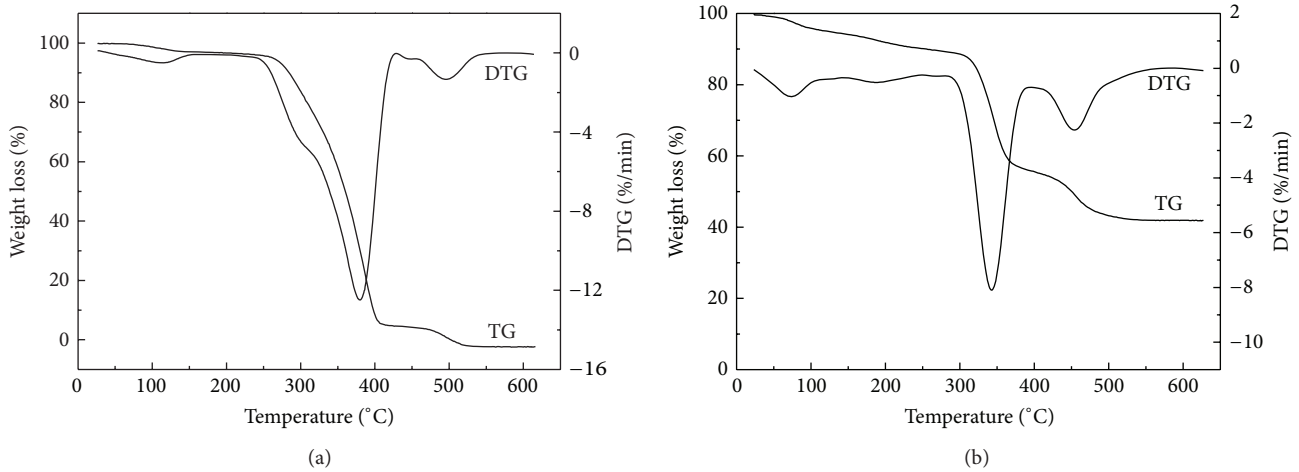

Figure 1: TG-DTG curves of the PS spheres (a) and the TiO_2/PS composite.

residual solvent at low temperature below 300°C. The major weight loss of about 90% between 300 and 400°C can be assigned to the thermal decomposition of the polystyrene, which was decomposed from long chain to shorter chain and then depolymerized into volatile monomers with low molecular weight. While, the third stage in the range of 400–500°C can be attributed to the combustion of the residual coke. With respect to the TiO_2/PS nanocomposite, it is found that PS spheres can be completely removed at 500°C (Figure 1(b)). Thus, 500°C was selected as the calcination temperature to prepare the macroporous TiO_2 photocatalyst. The weight content of TiO_2 in the TiO_2/PS nanocomposite is calculated to be 43.2%.

XRD are employed to characterize the crystallite structure of the synthesized TiO_2 catalysts. It can be seen from Figure 2(a) that the diffraction peaks of TiO_2 after being calcinated at 450°C can be indexed to anatase phase TiO_2 (JCPDS NO. 21-1272) and rutile phase TiO_2 (JCPDS NO. 21-1276), indicating that the sample calcined at 450°C is composed of bicrystalline phase. When the calcination temperature was increased to 500°C, all diffraction peaks can be indexed to pure anatase phase (JCPDS NO. 21-1272), and no characteristic peaks of other impurities can be detected. Thus, 500°C is a proper sintering temperature to prepare anatase phase macroporous TiO_2, which is in accordance with the TG-DTG analysis (Figure 1). The sharp diffraction peaks in Figure 2(b) illustrate the well crystallization of m-TiO_2 after the heat treatment. The crystallite size (D) was calculated to be about 10 nm according to the Scherrer formula $D = K\lambda/\beta\cos\theta$ [39], where K is a constant (shape factor, about 0.9), λ is the X-ray wavelength (0.15418 nm), β is the full-width at half-maximum, and θ is the diffraction angle. The values of β and θ were taken from TiO_2 (101) diffraction line.

TEM images of the PS spheres and m-TiO_2 are given in Figure 3. Figure 3(a) shows the TEM image of the PS spheres. The size of the PS spheres is about 278 nm, and the standard deviation of monodispersed spheres is less than 2.76%. This

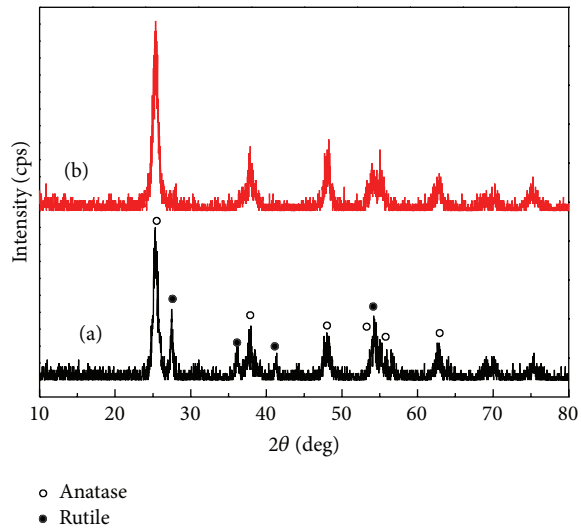

Figure 2: XRD patterns of TiO_2 prepared through calcining the TiO_2/PS composite at different temperatures: (a) 450°C and (b) 500°C.

indicates that the PS spheres are suitable to be employed as macroporous templates. As shown in Figure 3(b), the PS spheres are wrapped by TiO_2 nanoparticles before being sintered. Figure 3(c) shows the low-magnification TEM image of macroporous TiO_2 sintered at 500°C in air, from which macropores can be clearly seen, suggesting that PS spheres have been completely removed after calcination at 500°C in air. And the SEM image (Figure 3(e)) also demonstrates well-defined macroporous structure. The size of the hollow spheres is about 240 nm, which is smaller than the size of original PS spheres template, suggesting the significant shrinkage after the PS removal via calcination. Additionally, Figure 3(c) also illustrates that run-through-macropore network structure was formed. And the SEM images in Figure 3(e) further confirm that the macropores left by the templates are interconnective with neighboring hollow

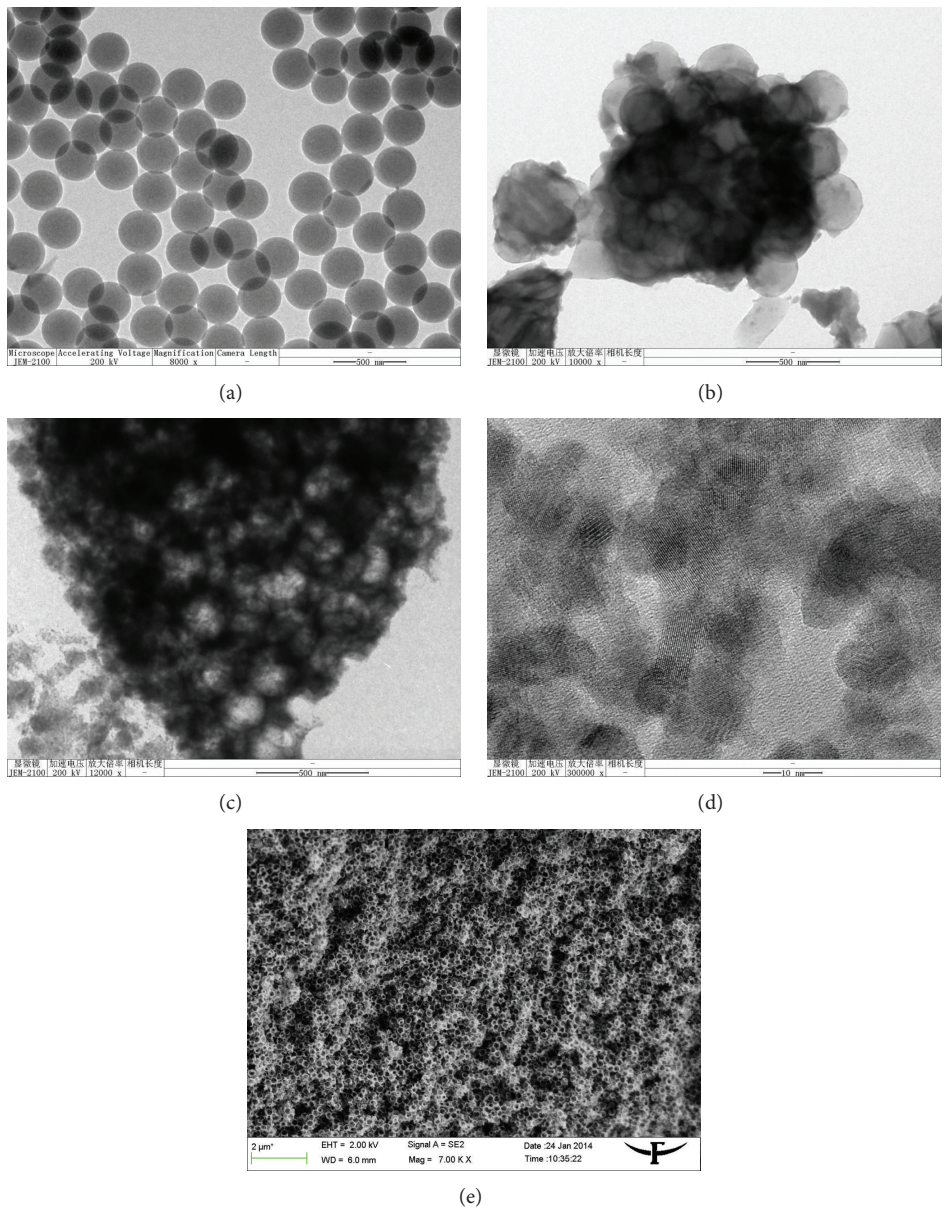

Figure 3: Low-magnification TEM images of (a) the PS spheres, (b) the TiO_2/PS composites, (c) the m-TiO_2 catalyst after calcination at 500°C, and the high-resolution TEM image (d) and SEM image (e) of the m-TiO_2 sample.

spheres. High-resolution TEM image (Figure 3(d)) displays that the crystalline size of TiO_2 nanoparticles is about 10 nm, which is in good agreement with the XRD analysis.

N_2 adsorption-desorption measurements were performed to investigate the textural properties of the macroporous TiO_2. The N_2 adsorption-desorption isotherms of r-TiO_2 and m-TiO_2 are shown in Figure 4. One can see that the isotherm of the r-TiO_2 is of typical type IV, characteristic of mesoporous materials, according to IUPAC classification. The adsorbed nitrogen volume for m-TiO_2 becomes steep in the P/P_0 range of 0.8–1.0, which indicates the presence of large macropores. Based on the Brunauer-Emmett-Teller (BET) equation, the specific surface areas of r-TiO_2 and m-TiO_2 were evaluated to be about 91.2 and 87.8 m^2/g, respectively.

3.2. Photocatalytic Activity Test. The photocatalytic activities of the prepared TiO_2 samples were examined through the photodegradation of RhB under UV light irradiation. The degradation efficiency was illustrated by the change of the RhB concentration during the photodegradation process and the results were shown in Figure 5. The photocatalytic results reveal that the photocatalytic activity of the macroporous TiO_2 was significantly improved as compared to that of the traditional TiO_2 nanoparticles. For the macroporous TiO_2, 92.63% of the RhB was decomposed after 2 h irradiation.

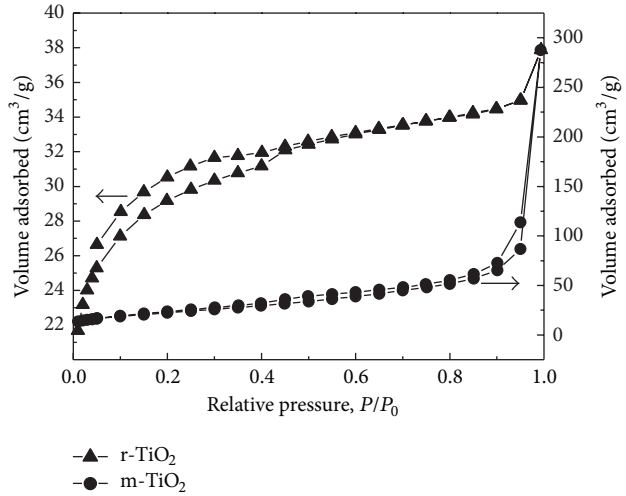

Figure 4: Nitrogen adsorption-desorption isotherms of the r-TiO_2 and m-TiO_2 after calcination at 500°C for 2 h.

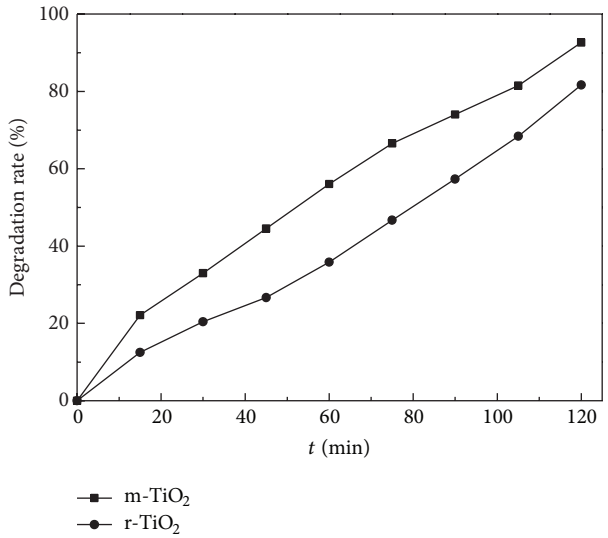

Figure 5: Degradation efficiency curves of RhB for the r-TiO_2 and m-TiO_2 after calcination at 500°C for 2 h.

However, as to the r-TiO_2 sample, the degradation percentage is only 81.66%. Here, the macroporous structure is believed to facilitate the transportation of reactant molecules and products through the interior space due to the run-through-macropore networks [40–43] and to favor the harvesting of exciting light due to enlarged surface area and multiple scattering within the porous framework [43, 44]. So the enhanced photoactivity of m-TiO_2 could be achieved.

4. Conclusions

In summary, macroporous TiO_2 photocatalyst was successfully synthesized via a simple sol-gel method using polystyrene spheres as sacrificial templates. The prepared macroporous TiO_2 exhibited higher photocatalytic activity than the TiO_2 sample through a template-free approach in catalyzing the degradation of RhB under UV light illumination. And the superior photocatalytic performance can be related to the run-through-macropore network structure. Considering the facile preparation and high photocatalytic activity, the macroporous TiO_2 materials display a good potential in the fields of environmental remediation and energy conversion and storage.

Conflict of Interests

The authors have no conflict of interests in relation to the instrumental companies directly or indirectly.

Acknowledgments

This work was supported by the National Natural Science Foundation of China (U1361119, 51174077), Specialized Research Fund for the Doctoral Program of Higher Education (20124116120002), the Education Department Key Programs for Science and Technology Research of He'nan Province (13A430336, 2011A480003).

References

[1] S. D. Richardson, C. S. Willson, and K. A. Rusch, "Use of rhodamine water tracer in the marshland upwelling system," *Ground Water*, vol. 42, no. 5, pp. 678–688, 2004.

[2] J. Ryu and W. Choi, "Substrate-specific photocatalytic activities of TiO_2 and multiactivity test for water treatment application," *Environmental Science and Technology*, vol. 42, no. 1, pp. 294–300, 2008.

[3] H. Cui, H. Liu, J. Shi, and C. Wang, "Function of TiO_2 lattice defects towards photocatalytic process: view of electronic driven force," *International Journal of Photoenergy*, vol. 2013, Article ID 364802, 16 pages, 2013.

[4] P. Chou, S. Matsui, K. Misaki, and T. Matsuda, "OH radical formation at distinct faces of rutile TiO_2 crystal in the procedure of photoelectrochemical water oxidation," *The Journal of Physical Chemistry C*, vol. 117, no. 45, pp. 23832–23839, 2013.

[5] R. Daghrir, P. Drogui, and D. Robert, "Modified TiO_2 for environmental photocatalytic applications: a review," *Industrial & Engineering Chemistry Research*, vol. 52, no. 10, pp. 3581–3599, 2013.

[6] H. Huang, H. Huang, P. Hu, X. Ye, and D. Y. C. Leung, "Removal of formaldehyde using highly active Pt/TiO_2 catalysts without irradiation," *International Journal of Photoenergy*, vol. 2013, Article ID 350570, 6 pages, 2013.

[7] R. Giovannetti, M. Zannotti, L. Alibabaeu, and S. Ferraro, "Equilibrium and kinetic aspects in the sensitization of monolayer transparent TiO_2 thin films with porphyrin dyes for DSSC applications," *International Journal of Photoenergy*, vol. 2014, Article ID 834269, 9 pages, 2014.

[8] B. Wang and L. L. Kerr, "Stability of CdS-coated TiO_2 solar cells," *Journal of Solid State Electrochemistry*, vol. 16, no. 3, pp. 1091–1097, 2012.

[9] S. Phanichphant, C. Liewhiran, K. Wetchakun, A. Wisitsoraat, and A. Tuantranont, "Flame-made Nb-doped TiO_2 ethanol and acetone sensors," *Sensors*, vol. 11, no. 1, pp. 472–484, 2011.

[10] L.-C. Jiang and W.-D. Zhang, "Electrodeposition of TiO_2 nanoparticles on multiwalled carbon nanotube arrays for hydrogen peroxide sensing," *Electroanalysis*, vol. 21, no. 8, pp. 988–993, 2009.

[11] V. Tajer-Kajinebaf, H. Sarpoolaky, and T. Mohammadi, "Synthesis of nanostructured anatase mesoporous membranes with photocatalytic and separation capabilities for water ultrafiltration process," *International Journal of Photoenergy*, vol. 2013, Article ID 509023, 11 pages, 2013.

[12] C. S. Guo, M. Ge, L. Liu, G. Gao, Y. Feng, and Y. Wang, "Directed synthesis of mesoporous TiO_2 microspheres: catalysts and their photocatalysis for bisphenol A degradation," *Environmental Science and Technology*, vol. 44, no. 1, pp. 419–425, 2010.

[13] Y.-C. Park, Y.-J. Chang, B.-G. Kum et al., "Size-tunable mesoporous spherical TiO_2 as a scattering overlayer in high-performance dye-sensitized solar cells," *Journal of Materials Chemistry*, vol. 21, no. 26, pp. 9582–9586, 2011.

[14] C. J. W. Ng, H. Gao, and T. T. Yang Tan, "Atomic layer deposition of TiO_2 nanostructures for self-cleaning applications," *Nanotechnology*, vol. 19, no. 44, Article ID 445604, 2008.

[15] Z. Bian, J. Zhu, F. Cao, Y. Huo, Y. Lu, and H. Li, "Solvothermal synthesis of well-defined TiO_2 mesoporous nanotubes with enhanced photocatalytic activity," *Chemical Communications*, vol. 46, no. 44, pp. 8451–8453, 2010.

[16] H. Z. Zhang, F. Dong, S. N. Zhai, X. J. Kang, and S. M. Fang, "Preparation of ordered TiO_2 macroporous membrane using PBMA colloid crystal as template," *Advanced Materials Research*, vol. 399–401, pp. 677–682, 2012.

[17] G. Q. Liu, Z. G. Jin, X. X. Liu, T. Wang, and Z. F. Liu, "Anatase TiO_2 porous thin films prepared by sol-gel method using CTAB surfactant," *Journal of Sol-Gel Science and Technology*, vol. 41, no. 1, pp. 49–55, 2007.

[18] H. Bala, Y. Yu, and Y. Zhang, "Synthesis and photocatalytic oxidation properties of titania hollow spheres," *Materials Letters*, vol. 62, no. 14, pp. 2070–2073, 2008.

[19] X. Zheng, Q. Kuang, K. Yan, Y. Qiu, J. Qiu, and S. Yang, "Mesoporous TiO_2 single crystals: facile shape-, size-, and phase-controlled growth and efficient photocatalytic performance," *ACS Applied Materials & Interfaces*, vol. 5, no. 21, pp. 11249–11257, 2013.

[20] Y. Dong, J. Chao, Z. Xie, X. Xu, Z. Wang, and D. Chen, "Highly ordered TiO_2 macropore arrays as trandparent photocatalysts," *Journal of Nanomaterials*, vol. 2012, Article ID 762510, 6 pages, 2012.

[21] P. Jiang, J. Cizeron, J. F. Bertone, and V. L. Colvin, "Preparation of macroporous metal films from colloidal crystals," *Journal of the American Chemical Society*, vol. 121, no. 34, pp. 7957–7958, 1999.

[22] M. Sadakane, T. Horiuchi, N. Kato, C. Takahashi, and W. Ueda, "Facile preparation of three-dimensionally ordered macroporous alumina, iron oxide, chromium oxide, manganese oxide, and their mixed-metal oxides with high porosity," *Chemistry of Materials*, vol. 19, no. 23, pp. 5779–5785, 2007.

[23] M. Davis, D. A. Ramirez, and L. J. Hope-Weeks, "Formation of three-dimensional ordered hierarchically porous metal oxides via a hybridized epoxide assisted/colloidal crystal templating approach," *Applied Materials & Interfaces*, vol. 5, no. 16, pp. 7786–7792, 2013.

[24] T. Kimura, N. Miyamoto, X. Meng, T. Ohji, and K. Kato, "Rapid fabrication of mesoporous titania films with controlled macroporosity to improve photocatalytic property," *Chemistry* , vol. 4, no. 9, pp. 1486–1493, 2009.

[25] X.-Y. Li, L.-H. Chen, Y. Li et al., "Self-generated hierarchically porous titania with high surface area: photocatalytic activity enhancement by macrochannel structure," *Journal of Colloid and Interface Science*, vol. 368, no. 1, pp. 128–138, 2012.

[26] R.-F. Zhang, J. Ye, and N.-B. Long, "Large-sized TiO_2/SiO_2 macroporous materials for photodegradation of organic compounds in water and air," *Advanced Materials Research*, vol. 306-307, pp. 1157–1161, 2011.

[27] L. Szymanski, P. Surolia, O. Byrne, K. R. Thampi, and C. Stubenrauch, "Porous "sponge-like" anatase TiO_2 via polymer templates: synthesis, characterization, and performance as a light-scattering material," *Colloid and Polymer Science*, vol. 291, no. 4, pp. 805–815, 2013.

[28] F. Z. Huang, D. H. Chen, X. L. Zhang, R. A. Caruso, and Y.-B. Cheng, "Dual-function scattering layer of submicrometer-sized mesoporous TiO_2 beads for high-efficiency dyesensitized solar cells," *Advanced Functional Materials*, vol. 20, no. 8, pp. 1301–1305, 2010.

[29] T. Yan, L. Li, G. Li, Y. Wang, W. Hu, and X. Guan, "Porous $SnIn_4S_8$ microspheres in a new polymorph that promotes dyes degradation under visible light irradiation," *Journal of Hazardous Materials*, vol. 186, no. 1, pp. 272–279, 2011.

[30] G. Cappelletti, "TiO_2 nanoparticles: traditional and novel synthetic methods for photocatalytic paint formulations," in *Nanoparticles: Properties, CLassification Characterization and Fabrication, S.L*, pp. 213–254, Nova Science Publishers, 2010.

[31] S. Yurdakal, B. S. Tek, O. Alagöz et al., "Photocatalytic selective oxidation of 5-(Hydroxymethyl)-2-furaldehyde to 2,5-Furandicarbaldehyde in water by using anatase, rutile, and brookite TiO_2 nanoparticles," *Sustainable Chemistry & Engineering*, vol. 1, no. 5, pp. 456–461, 2013.

[32] Q. Zhou, P. Dong, G.-Y. Yi, L.-X. Liu, and B.-Y. Cheng, "Preparation of TiO_2 inverse opal via a modified filling process," *Chinese Physics Letters*, vol. 22, no. 5, pp. 1155–1158, 2005.

[33] X.-D. Wang, P. Dong, and G.-Y. Yi, "Evaporation self-assembly method to fabricate high-quality polystyrene microsphere colloid crystal," *Acta Physica Sinica*, vol. 55, no. 4, pp. 2092–2098, 2006.

[34] X.-D. Wang, G.-Y. Yi, and Y. Liu, "Preparation of Al_2O_3 catalytic material with run-through-macropore network structure," *Chemical Journal of Chinese Universities*, vol. 30, no. 2, pp. 349–354, 2009.

[35] C. Wang, Z.-X. Deng, G. Zhang, S. Fan, and Y. Li, "Synthesis of nanocrystalline TiO_2 in alcohols," *Powder Technology*, vol. 125, no. 1, pp. 39–44, 2002.

[36] Y. Li, T. J. White, and S. H. Lim, "Low-temperature synthesis and microstructural control of titania nano-particles," *Journal of Solid State Chemistry*, vol. 177, no. 4-5, pp. 1372–1381, 2004.

[37] E. T. Soares, M. A. Lansarin, and C. C. Moro, "A study of process variables for the photocatalytic degradation of rhodamine B," *Brazilian Journal of Chemical Engineering*, vol. 24, no. 1, pp. 29–36, 2007.

[38] K. Byrappa, A. K. Subramani, S. Ananda, K. M. Lokanatha Rai, R. Dinesh, and M. Yoshimura, "Photocatalytic degradation of rhodamine B dye using hydrothermally synthesized ZnO," *Bulletin of Materials Science*, vol. 29, no. 5, pp. 433–438, 2006.

[39] H. P. Klong and L. E. Alexander, *X-Ray Diffraction Procedures for Crystalline and Amorphous Solids*, Wiley, New York, NY, USA, 1954.

[40] Z.-Y. Yuan and B.-L. Su, "Insights into hierarchically meso-macroporous structured materials," *Journal of Materials Chemistry*, vol. 16, no. 7, pp. 663–677, 2006.

[41] C. M. A. Parlett, K. Wilson, and A. F. Lee, "Hierarchical porous materials: catalytic applications," *Chemical Society Reviews*, vol. 42, pp. 3876–3893, 2013.

[42] J. G. Yu, S. W. Liu, and H. G. Yu, "Microstructures and photoactivity of mesoporous anatase hollow microspheres fabricated by fluoride-mediated self-transformation," *Journal of Catalysis*, vol. 249, no. 1, pp. 59–66, 2007.

[43] G. Kaune, M. Memesa, R. Meier et al., "Hierarchically structured titania films prepared by polymer/colloidal templating," *ACS Applied Materials and Interfaces*, vol. 1, no. 12, pp. 2862–2869, 2009.

[44] X. C. Wang, J. C. Yu, C. Ho, Y. D. Hou, and X. Z. Fu, "Photocatalytic activity of a hierarchically macro/mesoporous titania," *Langmuir*, vol. 21, no. 6, pp. 2552–2559, 2005.